FEBS Letters 588 (2014) 4369–4374

journal homepage: www.FEBSLetters.org

A switch-like dynamic mechanism for the initiation of replicative senescence

Qing-He Zhang, Xiao-Jun Tian, Feng Liu *, Wei Wang *

National Laboratory of Solid State Microstructures and Department of Physics, Nanjing University, Nanjing 210093, China

ARTICLE INFO

Article history:
Received 16 May 2014
Accepted 15 September 2014
Available online 12 October 2014

Edited by Paul Bertone

Keywords:
Replicative senescence
Telomere shortening
Regulatory network
Bistable switch
p53 activation

ABSTRACT

Telomeres are specialized structures protecting chromosomes against genome instability. Telomeres shorten with cell division, and replicative senescence is induced when telomeres are badly eroded. Whereas TRF2 (telomeric-repeat binding factor 2), ATM (ataxia telangiectasia mutated) and p53 have been identified involved in senescence induction, how it is triggered remains unclear. Here, we propose an integrated model associating telomere loss with senescence trigger. We characterize the dynamics of telomere shorting and the p53-centered regulatory network. We show that senescence is initiated in a switch-like manner when both the shortest telomere becomes uncapped and the TRF2-ATM-p53-Siah1 positive feedback loop is switched on. This work provides a coherent picture of senescence induction in terms of telomere shortening and p53 activation.
© 2014 Federation of European Biochemical Societies. Published by Elsevier B.V. All rights reserved.

1. Introduction

Telomeres are specialized chromatin structures that cap the ends of linear chromosomes and protect them from deterioration, end-to-end fusion, and being recognized as damaged DNA [1]. The function of a telomere depends on its length, specific DNA structure and engagement of telomere proteins. Either end of a chromosome has repetitive nucleotide sequences (like 5′-TTAGGG-3′ in mammals). Because conventional DNA polymerases are unable to replicate the very ends of chromosomes (i.e., end-replication problem), telomeres in normal human somatic cells shorten with each round of DNA replication [2]. Telomere DNA forms a lariat structure (called t-loop) by invading of the 3′-overhang into the duplex telomeric repeat array [3]. Telomeric repeats provide binding sites for the telomere-specific protein complex, shelterin, which consists of TRF1 (telomeric-repeat binding factor 1), TRF2, POT1 (protection of telomeres protein 1), RAP1, TIN2, and TPP1 in mammals [4]. TRF1 and TRF2 directly bind the double-stranded telomere repeats, while POT1 directly binds the single-stranded 3′-overhang; they are interconnected by the other three components. Shelterin is indispensable for mediating telomere end-capping. Specifically, TRF2 can modulate t-loop formation [3] and prevent the ATM (ataxia telangiectasia mutated) kinase from initiating DNA damage responses at functional telomeres [5].

Telomeres can switch between two states: capped and uncapped, and the probability that a telomere becomes uncapped rises as its length shortens [6]. Capping is defined as preserving the physical integrity of the telomere, involving the t-loop structure and recruitment of enough shelterin complexes [4]. Uncapping is characterized by loss of 3′-overhang, telomere fusion-induced chromosome instability and activated DNA damage signaling. In telomerase-negative cells, if a telomere remains uncapped persistently, either senescence or apoptosis is triggered to prevent propagation of damaged DNA [7]. Replicative senescence is characterized by irreversible cell cycle exit with sustained metabolic activity. Apoptosis provides an efficient way to kill irreparably damaged cells.

The tumor suppressor p53 has a critical role in inducing senescence and apoptosis by regulating expression of target genes [8]. As an endogenous DNA damage, sustained telomere uncapping activates ATM and p53. Moreover, p53 is not only a downstream effector of the damage signaling, but also functions upstream to regulate TRF2. p53 can downregulate TRF2 levels through Siah1 (seven in absentia homolog 1), a p53-inducible E3 ubiquitin ligase. Siah1 targets TRF2 for ubiquitination and proteasomal degradation [9]. That is, the TRF2-ATM-p53-Siah1 positive feedback loop can amplify the cellular response initiated by uncapped telomeres [10]. Moreover, p53 isoforms, such as Δ133p53 and p53β, and its

* Corresponding authors. Address: Department of Physics, Nanjing University, Nanjing 210093, China. Fax: +86 25 83595535.
E-mail addresses: fliu@nju.edu.cn (F. Liu), wangwei@nju.edu.cn (W. Wang).

http://dx.doi.org/10.1016/j.febslet.2014.09.043
0014-5793/© 2014 Federation of European Biochemical Societies. Published by Elsevier B.V. All rights reserved.

family members, p63 and p73, are also regulators of cellular senescence [11].

The underlying mechanism for the induction and maintenance of senescence is less well understood. Whereas much attention has focused on the dynamics of telomere shortening and its correlation with senescence induction, few studies explored the dynamics of the p53 network during the initiation of replicative senescence. It is generally assumed that senescence is triggered when the shortest telomere reaches a critical length (i.e., the Hayflick limit) [12]. But how is it determined? The cell fate is closely associated with the (un)capping status of telomeres, and it seems essential to probe how replicative senescence is coherently triggered by coupling telomere shorting with DNA damage signaling.

Motivated by the above considerations, we build a minimal model correlating telomere shortening with p53 activation to clarify the mechanism for senescence induction in human diploid fibroblasts. We characterize both the temporal evolution of telomere length and the dynamics of the TRF2-ATM-p53-Siah1 and p53-Mdm2 feedback loops. We take into account three mechanisms contributing to telomere shortening. When telomeres are critically eroded, the TRF2-ATM-p53-Siah1 loop is switched on, contributing to downregulation of TRF2. This further leads to full activation of ATM and p53. Meanwhile, the concentration of phosphorylated p53 rises from a low to high level, so that senescence is triggered. The p53 dynamics exhibit a switch-like behavior, subserving the maintenance and reinforcement of senescence.

2. Materials and methods

2.1. Modeling telomere loss

We develop a stochastic algorithm to simulate the temporal evolution of the length of each telomere in a cell (the detailed description is presented in the Supplemental Material). There are 46 chromosomes and 92 telomeres in human fibroblasts. They can be divided into three categories in terms of initial length, separately comprising 30, 30, and 32 telomeres [13]. Their initial length is assumed to obey a normal distribution with the mean of 9, 7, and 11 kb, respectively, and the variance of 1 kb. The telomeres are considered in pairs for each chromosome, i.e., whether a telomere at one end of the chromosome is shortened after cell division depends on what occurs on the telomere at the other end. Similar to [14], we take into account three mechanisms underlying telomere loss at each division, i.e., incomplete end replication [2], processing of C-rich strands by exonuclease [15], and unrepaired single-strand breaks caused by oxidative stress [16]. The contribution of each mechanism to telomere shortening is illustrated in Fig. S1A, and the estimates for telomere loss after each division are presented in Fig. S1B. Note that the minimal telomere length after each division is taken as the input to the p53 network.

2.2. p53 network

The telomere dysfunction is detected by a regulatory signaling network including TRF2, ATM and p53. We construct a minimal model to characterize how eroded telomeres activate p53, focusing on the TRF2-ATM-p53-Siah1 and p53-Mdm2 loops (Fig. 1). TRF2 is mainly localized in the nucleus. There are three forms of TRF2: $TRF2_m$, $TRF2_{db}$ and $TRF2_{df}$. $TRF2_m$ denotes TRF2 monomers. $TRF2_{db}$ refers to functional TRF2 dimers that bind the telomeric repeats to rebuild the t-loop structure, preventing ATM from autophosphorylation [17], whereas $TRF2_{df}$ represents free, unbound dimers. With telomere shortening, the number of binding sites for TRF2 on telomeres decreases gradually, and thus the amount of $TRF2_{db}$ declines. The relationship between the concentrations of $TRF2_{db}$ and $TRF2_{df}$ and the telomere length is derived in the Supplemental Method. In our model, the information about the telomere state is transmitted to the p53 signaling network via TRF2.

The binding of TRF2 dimers to telomeres inhibits the phosphorylation of ATM on Ser1981 [17], an early step in its activation. ATM exists predominantly as dimers in unstressed cells. Dysfunctional telomeres promote the conversion of ATM from dimers to inactive monomers and to active, phosphorylated monomers. Phosphorylated ATM (ATM_p) further accelerates the activation of ATM via intermolecular autophosphorylation [18]. The total level of ATM is assumed to be constant since ATM is mainly regulated post-translationally. The phosphorylation and dephosphorylation of ATM are taken as enzyme-catalyzed reactions and are assumed to follow the Michaelis–Menten kinetics [19].

Activated ATM phosphorylates p53 and Mdm2, repressing their interaction and promoting the degradation of Mdm2. Consequently, p53 is stabilized and activated [20]. Phosphorylated p53 ($p53_p$) induces the expression of *mdm2*, whereas Mdm2 targets p53 for proteasomal degradation; this negative feedback loop ensures that p53 has a very low level under unstressed conditions. $p53_p$ transactivates the expression of *siah1*, and Siah1 targets $TRF2_{df}$ for proteasome-mediated degradation [9]. The transcription of genes by p53 is characterized by Hill function, and the Hill coefficient is set to 4 given the cooperativity of the tetrameric form of p53 as a transcription factor [21]. Since we concern only the initiation of senescence, for simplicity we do not consider the downstream targets of p53 that contribute to maintenance of senescence, including p21.

2.3. Method

The details of model construction are presented in Supplemental Material. The telomere shorting with cell division is simulated stochastically, whereas the concentration of each species is represented by a state variable in deterministic rate equations ([...] represents the concentration of species throughout the text). The initial values of variables and standard parameter values are presented in Supplemental Table S1 and S2, respectively. The time step for integrating ordinary differential equations is 0.01 min. The cell is assumed to divide every 3 days.

3. Results

3.1. Dynamics of the telomere length and the p53 network

We keep track of the lengths of 92 telomeres; they shorten with cell replication. We illustrate the temporal evolution of the minimal telomere length L_m in a cell (Fig. 2A). As the number of cell divisions rises, L_m gradually decreases in a stochastic way; in this example, the cell stops dividing after the 56th division, where L_m reaches 1 kb. After that, the cell becomes senescent. This result agrees with the experimental observation [13]. We also show the distributions of telomere length among 92 telomeres at the beginning and at the end of replicative lifespan in the inset. The distribution shifts leftward and telomere lengths are more widely distributed in the senescent state. Whereas there is a large variability in telomere length, senescence is triggered when the minimum telomere length is sufficiently short and the telomere is badly eroded, as shown later.

Furthermore, we display the distribution of L_m at the end of replicative lifespan among 2000 cells (Fig. 2B). Clearly, most of L_m is located around 1 kb, whereas L_m in some cells can be much less than 1 kb. In fact, L_m is longer than 1.1 kb immediately before the senescent state, but after the replication, L_m may drop to various extents because of three mechanisms: the loss is uniformly

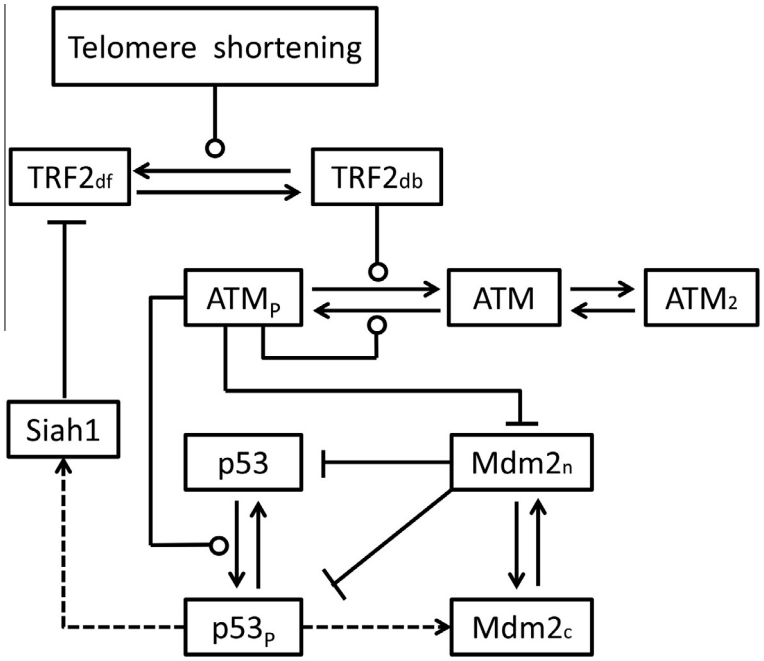

Fig. 1. Schematic depiction of the model. When bound to telomeres, TRF2 dimers interact with ATM preventing its autophosphorylation and activation. When telomeres are badly eroded, ATM is activated, converting from dimer (ATM_2) to monomer and phosphorylated monomer (ATM_p). Subsequently, p53 is stabilized and activated by phosphorylation. Phosphorylated p53 ($p53_p$) transactivates *mdm2* and *siah1*. Mdm2 targets p53 for degradation. Siah1 targets TRF2 for ubiquitination and degradation. The TRF2-ATM-p53-Siah1 positive feedback loop has a critical role in inducing senescence. Note that the minimum telomere length is taken as an input to the regulatory network through affecting the $TRF2_{db}$ level. Dashed lines denote gene expression by p53, and solid arrowed lines represent the transition between states. The circle- and bar-headed lines denote the promotion of state transition and of protein degradation, respectively.

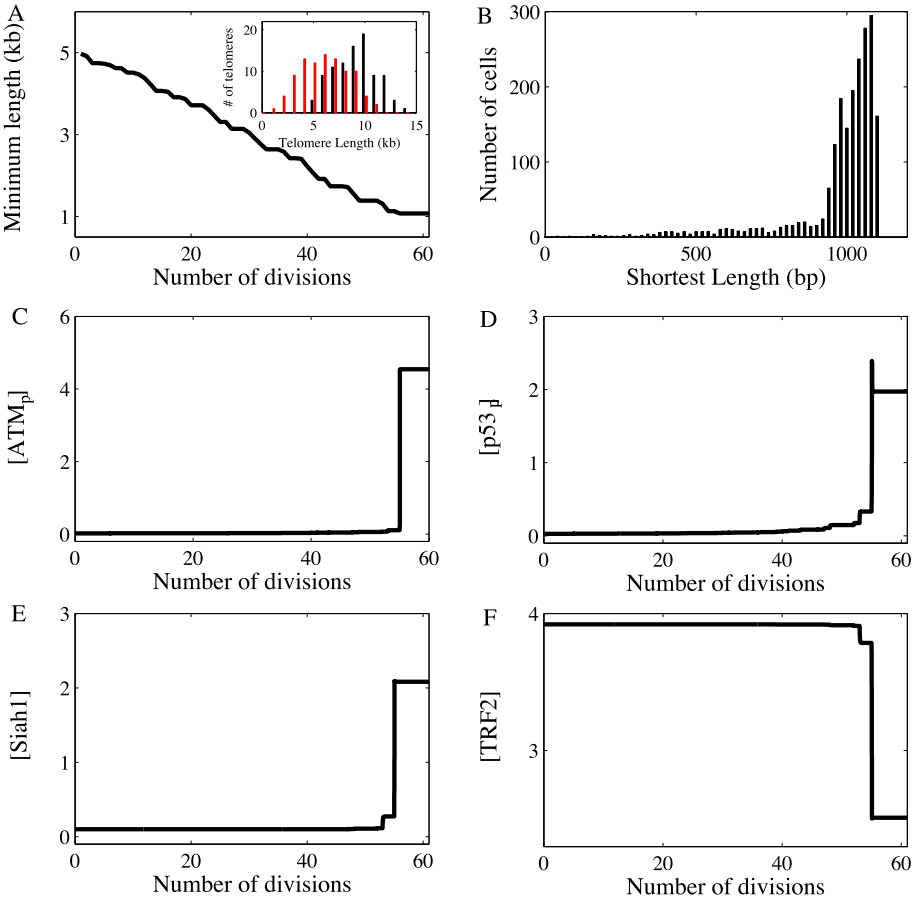

Fig. 2. Dynamics of telomere length and key proteins. (A) The shortest telomere length L_m in a cell versus the number of cell divisions. The inset shows the distributions of telomere length among 92 telomeres at the beginning (*black*) and at the senescent state (*red*). (B) The distribution of the minimum telomere length at the end of replicative lifespan among 2000 cells. (C–F) Time courses of the levels of ATM_p, $p53_p$, Siah1 and TRF2 corresponding to telomere shortening in panel *A*.

distributed between 10 and 110 nucleotides (nt) because of the end-replication problem, the loss due to C-strand processing obeys a Poisson distribution with a mean of 155 nt, or the loss due to unrepaired single-strand breaks caused by oxidative stress is uniformly distributed between 0 and 1000 nt (see the details in Supplemental Method). The resulting shortening may make L_m widely distributed. This result also implies that it is unreasonable to preset a minimum telomere length for senescence initiation at the population level.

In the same case as in Fig. 2A, [ATM_p], [$p53_p$] and [Siah1] stay at low levels throughout the first 56 divisions, whereas the total amount of TRF2, [TRF2], remains relatively high (Fig. 2C–F). Although telomeres shorten with each round of DNA replication, p53 remains inactive before the 45th division and $p53_p$ accumulates gradually after that. Consequently, Siah1 is induced by p53 to downregulate TRF2, which in turn leads to enhanced activity of p53. At the 56th division, ATM and p53 are fully activated and their concentrations switch from low to relatively high levels. That is, p53 is activated in a switch-like manner. Meanwhile, [TRF2] drops to an intermediate level. Activated p53 will induce expression of target genes such as p21 to initiate and maintain senescence. These results highlight the importance of associating telomere shortening with p53 activation when trying to reveal the dynamic mechanism for senescence induction. It is unnecessary to preset a critical promoter length for senescence initiation because it follows the full activation of p53.

3.2. Initiation of replicative senescence is governed by a bistable switch

To systematically explore how the concentrations of proteins depend on the telomere state, we show the bifurcation diagrams of the steady-state levels of ATM_p, $p53_p$, Siah1 and TRF2 versus telomere length L (Fig. 3). There are two saddle-node bifurcation points, SN1 (left) and SN2 (right), in the diagrams. As the telomere length is decreased until 1.1 kb, [ATM_p], [$p53_p$], and [Siah1] stay in the lower state, whereas [TRF2] is in the upper state. [ATM_p], [$p53_p$], and [Siah1] are kept in the upper state when $L < 1.1$ kb. That is, the cell enters the senescent state. Since the telomere length cannot be restored to exceed 7 kb under normal physiological conditions, [ATM_p], [$p53_p$], and [Siah1] cannot switch from the upper to lower state; this ensures that replicative senescence is irreversible. That is, the senescent cell exits the cell cycle permanently. Therefore, once the lower threshold is reached, the senescent state is triggered and maintained. Taken together, here we propose that replicative senescence can be triggered in a switch-like manner. The two threshold lengths have practical implications. The lower threshold length determines the Hayflick limit. The upper threshold length decides how long the minimal telomere of the senescent cell should be extended such that the cell can resume proliferation in the presence of active telomerase. This awaits experimental validation.

Notably, the TRF2-ATM-p53-Siah1 positive feedback is responsible for the bistable switch underlying senescence induction. A critical uncapping state will be reached to activate the core ATM-p53 pathway once telomeres are badly eroded. In simulations, we assume that a single telomere is sufficient to stir up the concentrations of involved proteins in the nucleus. That is, among 92 telomeres, the one that first reaches the critical length can trigger the bistable switch. This is consistent with the observation that to induce senescence, the minimum telomere length should be less than 1–2 kb [13]. Collectively, here we propose that the components of the p53 network undergo switch-like dynamics, controlling initiation and maintenance of replicative senescence.

3.3. Dynamics of telomere shortening at the population level

The above results demonstrate how the bistable switch is triggered to induce senescence in a cell. To further illustrate the stochasticity in cell proliferation, we show temporal evolution of the fraction of dividing cells among 1000 cells (Fig. 4A). The fraction first decreases very slowly, then falls abruptly around the 50th division, and finally drops with a decreasing rate to 0 around the 85th division. These results suggest that the Hayflick limit is different in distinct cells because of the heterogeneity between cells and stochastic shortening of telomeres.

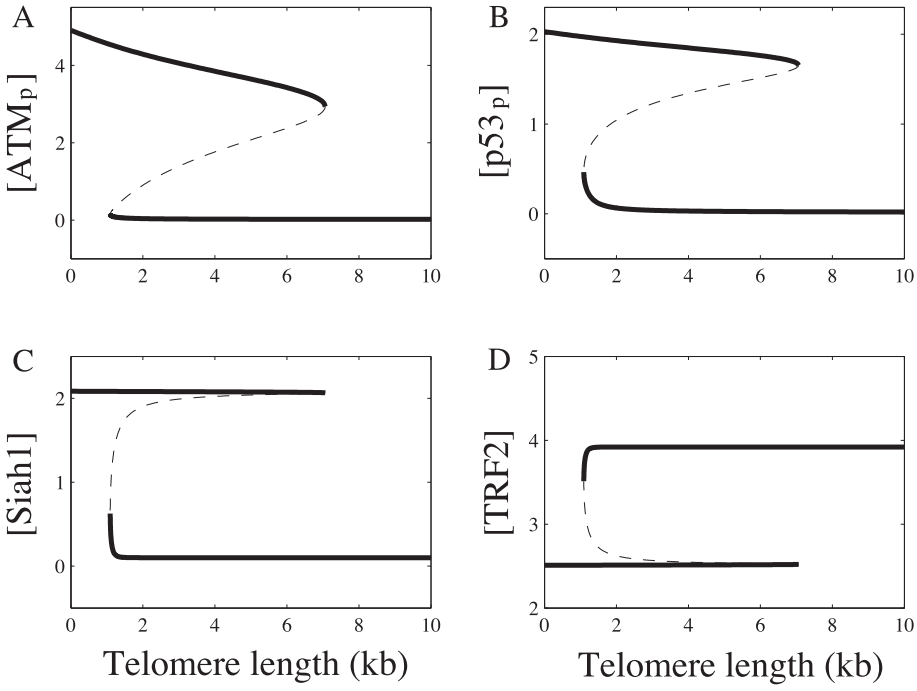

Fig. 3. Bistable switch underlying protein dynamics. Shown are bifurcation diagrams of the steady-state levels of ATM_p, $p53_p$, Siah1 and TRF2 as a function of fixed telomere length. The stable and unstable steady states are denoted by solid and dashed lines, respectively.

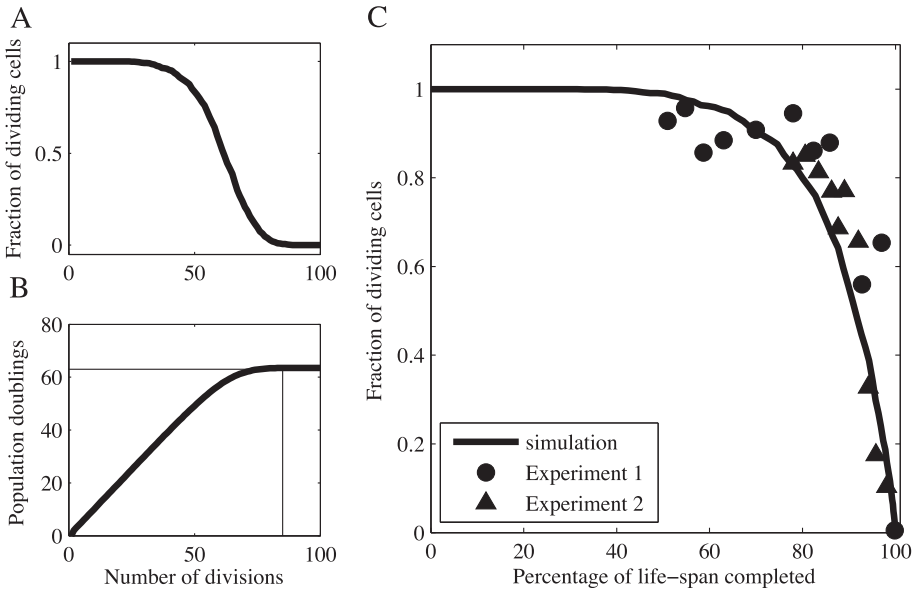

Fig. 4. Telomere shorting at the population level. (A) Fraction of dividing cells versus the number of cell divisions. We keep track of 1000 cells through their proliferating life. (B) The number of population doublings (PDs) versus the number of cell divisions. Here, cells achieve 63 population doublings before senescence, in agreement with the experimental data of 62 PD. (C) Fraction of dividing cells versus the percentage of lifespan completed. The experimental data from Ref. [22] are represented by circles and strangles, compared to the simulation results denoted by solid line.

Experimentally, it is more common to analyze telomere shortening during subsequent passage of human fibroblast cultures, and several measures were developed to characterize this process. For example, replicative lifespan depends on the culture size, which can be calculated by cumulative population doublings [22], i.e., $\mathrm{PD} = \log_2(D/D_0)$, where D and D_0 are separately the densities of cells at harvesting and upon seeding [13]. It is also equivalently defined as $\mathrm{PD} = \log_2(N/N_0)$, where N and N_0 are the number of cells at harvesting and at the beginning, respectively. The number of cells at the $(i+1)$th generation is $N(i+1) = 2F(i)N(i) + (1 - F(i))N(i)$, where $F(i)$ is the fraction of dividing cells at the ith generation, as shown in Fig. 4A. $F(i)N(i)$ is the number of dividing cells, whereas $(1 - F(i))N(i)$ is the number of senescent cells. We plot the population doublings versus the number of cell divisions in Fig. 4B.

At first only few cells become senescent, and $N(i)$ is approximately equal to $2^{i-1}N_0$. That is, the number of population doublings is quite equivalent to that of cell divisions, N_d. As N_d approaches 60, about 50% of cells become senescent. Since then, the value of population doublings is increasingly smaller than N_d. When N_d equals 85, all cells are senescent, and the maximum population doubling is 63. These results are in good agreement with experimental data [13].

Furthermore, the fraction of dividing cells as a function of the percentage of lifespan completed is shown in Fig. 4C. Remarkably, the simulation data provide a good fit to the experimental data from two independent cultures of human fibroblast strains [22]. A prominent feature is a rapid decline in the fraction of dividing cells during the period from 50% to 100% of lifespan completed. Taken together, the simulation results are quantitatively consistent with experimental data at the population level. This indicates that the present work provides an accurate characterization of dynamics of telomere shortening.

4. Discussion

Functional telomeres protect chromosomes from deterioration, end-to-end fusion, and recombination. Telomeres shorten gradually with cell division, and replicative senescence occurs when telomeres are badly eroded. We used a hybrid model to simulate the telomere loss and the dynamics of the p53 network. We consider three mechanisms contributing to telomere shortening. We found that the initiation of replicative senescence resembles a bistable switch, involving the full activation of ATM and p53. The bistable switch is trigged once the minimum telomere length reaches a threshold. The simulation results are well consistent with experimental data, such as cell senescence at 63 PD (Fig. 4B) and the faction of dividing cells rapidly declining during the period from 50% to 100% of lifespan completed (Fig. 4C). This work also provides a theoretical explanation for the Hayflick limit.

The switching mechanism for senescence induction may represent a flexible and robust mechanism. After each round of cell division, a new set of telomere lengths of daughter cells is checked; if the concentration of p53 sharply rises to high levels, the cells become senescent and stop dividing (Fig. 5). Otherwise, the cells further proliferate until senescence is induced. It is the hysteresis property of the bistable switch that ensures a reliable cell-fate decision by preventing the cells from stochastically flipping between different fates around the threshold. This mechanism plays a role in a wide variety of systems, such as mitosis commitment [23] and epithelial to mesenchymal transition [24].

Previous models of replicative senescence have assumed that cell cycle exit is triggered by the shortest or average telomere length past a critical point [14,25–27], or by a presumptive probability function of uncapping [28]. In the current work, we suggest that the direct trigger of replicative senescence is a bistable switch governed by the TRF2-ATM-p53-Siah1 loop. Notably, we showed that a single telomere can switch the cellular outcome from proliferation to senescence. Among 92 telomeres of a cell, the first one that reaches the critical length is able to activate the bistable switch and then trigger replicative senescence. We provide a reasonable explanation for the opinion that the shortest telomere correlates better with the remaining proliferative capacity of cells.

Finally, we note that the model ignored several factors involved in senescence regulation. We did not explicitly consider the transition dynamics between the capping and uncapping states, which involves the action of TRF1. TRF1 is able to loop, bend, and pair telomeric repeat arrays [3,29,30]; currently, how exactly TRF1 works is not well understood. We also did not consider the activation of ATR due to POT1 unbinding telomeres [5]. The

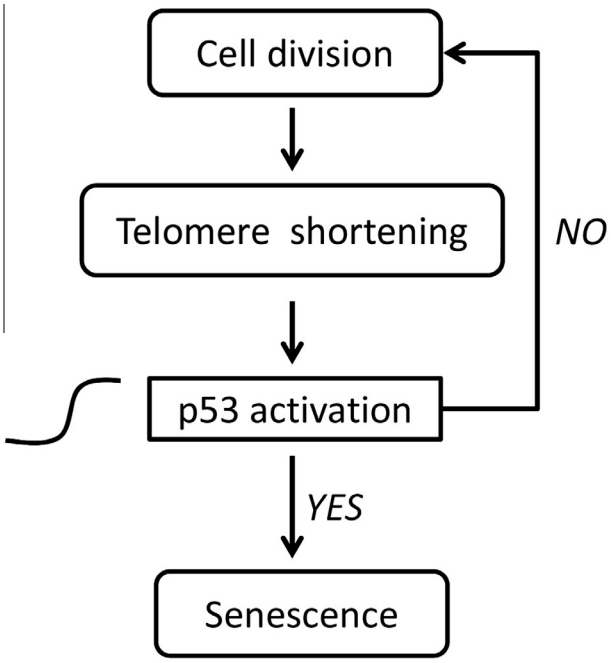

Fig. 5. Replicative senescence is triggered by p53 activation in a switch-like manner.

POT1-ATR-p53 pathway adds another level of complexity to regulation of p53 dynamics. It is important to add these factors to the model when more experimental data are available. Moreover, it would be interesting to extend the current model by considering telomerase and downstream effectors of p53 for senescence.

Conflict of interest

None of the authors has any potential conflicts of interest.

Acknowledgments

This work was supported by the 973 program of China (No. 2013CB834104), National Natural Science Foundation of China (Nos. 11175084 and 31361163003), and PAPD.

Appendix A. Supplementary data

Supplementary data associated with this article can be found, in the online version, at http://dx.doi.org/10.1016/j.febslet.2014.09.043.

References

[1] O'Sullivan, R.J. and Karlseder, J. (2010) Telomeres: protecting chromosomes against genome instability. Nat. Rev. Mol. Cell Biol. 11, 171–181.
[2] Olovnikov, A.M. (1996) Telomeres, telomerase, and aging: origin of the theory. Exp. Gerontol. 31, 443–448.
[3] Griffith, J.D., Comeau, L., Rosenfield, S., Stansel, R.M., Bianchi, A., et al. (1999) Mammalian telomeres end in a large duplex loop. Cell 97, 503–514.
[4] de Lange, T. (2005) Shelterin: the protein complex that shapes and safeguards human telomeres. Genes Dev. 19, 2100–2110.
[5] Denchi, E.L. and de Lange, T. (2007) Protection of telomeres through independent control of ATM and ATR by TRF2 and POT1. Nature 448, 1068–1071.
[6] Blackburn, E.H. (2000) Telomere states and cell fates. Nature 408, 53–56.
[7] Lechel, A., Satyanarayana, A., Ju, Z., Plentz, R.R., Schaetzlein, S., et al. (2005) The cellular level of telomere dysfunction determines induction of senescence or apoptosis in vivo. EMBO Rep. 6, 275–281.
[8] Feng, Z., Lin, M. and Wu, R. (2011) The regulation of aging and longevity: a new and complex role of p53. Genes Cancer 2, 443–452.
[9] Fujita, K., Horikawa, I., Mondal, A.M., Jenkins, L.M., Appella, E., et al. (2010) Positive feedback between p53 and TRF2 during telomere-damage signalling and cellular senescence. Nat. Cell Biol. 12, 1205–1212.
[10] Horikawa, I., Fujita, K. and Harris, C.C. (2011) P53 governs telomere regulation feedback too, via TRF2. Aging 3, 26–32.
[11] Rufini, A., Tucci, P., Celardo, I. and Melino, G. (2013) Senescence and aging: the critical roles of p53. Oncogene 32, 5129–5143.
[12] Hayflick, L. and Moorhead, P.S. (1961) The serial cultivation of human diploid cell strains. Exp. Cell Res. 25, 585–621.
[13] Martens, U.M., Chavez, E.A., Poon, S.S., Schmoor, C. and Lansdorp, P.M. (2000) Accumulation of short telomeres in human fibroblasts prior to replicative senescence. Exp. Cell Res. 256, 291–299.
[14] Proctor, C.J. and Kirkwood, T.B. (2002) Modelling telomere shortening and the role of oxidative stress. Mech. Ageing Dev. 123, 351–363.
[15] Wellinger, R.J., Ethier, K., Labrecque, P. and Zakian, V.A. (1996) Evidence for a new step in telomere maintenance. Cell 85, 423–433.
[16] von Zglinicki, T. (2002) Oxidative stress shortens telomeres. Trends Biochem. Sci. 27, 339–344.
[17] Karlseder, J., Hoke, K., Mirzoeva, O.K., Bakkenist, C., Kastan, M.B., et al. (2004) The telomeric protein TRF2 binds the ATM kinase and can inhibit the ATM-dependent DNA damage response. PLoS Biol. 2, E240.
[18] Bakkenist, C.J. and Kastan, M.B. (2003) DNA damage activates ATM through intermolecular autophosphorylation and dimer dissociation. Nature 421, 499–506.
[19] Zhang, X.P., Liu, F. and Wang, W. (2011) Two-phase dynamics of p53 in the DNA damage response. Proc. Natl. Acad. Sci. U.S.A. 108, 8990–8995.
[20] Prives, C. (1998) Signaling to p53: breaking the MDM2-p53 circuit. Cell 95, 5–8.
[21] Jeffrey, P.D., Gorina, S. and Pavletich, N.P. (1995) Crystal structure of the tetramerization domain of the p53 tumor suppressor at 1.7 angstroms. Science 267, 1498–1502.
[22] Harley, C.B. and Goldstein, S. (1980) Retesting the commitment theory of cellular aging. Science 207, 191–193.
[23] Sha, W., Moore, J., Chen, J., Lassaletta, A.D., Yi, C.S., et al. (2003) Hysteresis drives cell-cycle transitions in *Xenopus laevis* egg extracts. Proc. Natl. Acad. Sci. U.S.A. 100, 975–980.
[24] Tian, X.J., Zhang, H. and Xing, J. (2013) Coupled reversible and irreversible bistable switches underlying TGFβ-induced epithelial to mesenchymal transition. Biophys. J. 105, 1079–1089.
[25] Arino, O., Kimmel, M. and Webb, G.F. (1995) Mathematical modeling of the loss of telomere sequences. J. Theor. Biol. 177, 45–57.
[26] Rubelj, I. and Vondracek, Z. (1999) Stochastic mechanism of cellular aging – abrupt telomere shortening as a model for stochastic nature of cellular aging. J. Theor. Biol. 197, 425–438.
[27] Tan, Z. (1999) Telomere shortening and the population size-dependency of life span of human cell culture: further implication for two proliferation-restricting telomeres. Exp. Gerontol. 34, 831–842.
[28] Proctor, C.J. and Kirkwood, T.B. (2003) Modelling cellular senescence as a result of telomere state. Aging Cell 2, 151–157.
[29] Bianchi, A., Smith, S., Chong, L., Elias, P. and de Lange, T. (1997) TRF1 is a dimer and bends telomeric DNA. EMBO J. 16, 1785–1794.
[30] Bianchi, A., Stansel, R.M., Fairall, L., Griffith, J.D., Rhodes, D. and de Lange, T. (1999) TRF1 binds a bipartite telomeric site with extreme spatial flexibility. EMBO J. 18, 5735–5744.

Supplementary Material

A switch-like dynamic mechanism for the initiation of replicative senescence

Qing-He Zhang, Xiao-Jun Tian, Feng Liu and Wei Wang

In this study, we aim to reveal the dynamic mechanism for the initiation of replicative senescence. We built a hybrid model, characterizing telomere shortening and the p53-centered regulatory network. The details of the model are presented in Supplemental Method. The initial value of each variable and parameter values are listed in Supplemental Table S1 and S2, respectively.

Supplemental Method: Model construction

1. Telomere shortening

There are 46 chromosomes and 92 telomeres in human diploid fibroblasts. The length of 92 telomeres initially obeys a normal distribution and then shortens with cell division. We simulate the telomere shortening in a similar manner to that in [1]. Three main mechanisms contribute to telomere loss during cell proliferation. Because DNA polymerase requires a labile primer to initiate unidirectional 5'-3' synthesis, some bases at the 3' end of each template strand are not copied, which brings the widely recognized end-replication problem [2]. The action of a C-strand-specific exonuclease [3] and unrepaired single-strand breaks caused by oxidative stress [4] also have a critical role in telomere shortening. The telomeres must be considered in pairs: how and whether a telomere at one end of the chromosome is shortened after cell division depends on what happens to the telomere at the other end of the chromosome. The contribution of each mechanism to telomere loss is illustrated in Fig. S1A, and the quantitative telomere loss is estimated in Fig. S1B.

The amount of telomere loss caused by incomplete end-replication is represented by x, depending on where the last primer is located. x is taken as an integer uniformly distributed between 10 and 110 nucleotides (nt) (i.e., primer RNA (8~12 nt) + the minimum Okazaki fragment (100 nt)). Whether a telomere shortens due to incomplete end-replication depends on the chromosome arm on which it is located and on whether the daughter telomere is formed from the leading or lagging strand of the parent telomere.

A

Case	q arm p arm	Average length	Average loss
1) End-replication problem x=amount lost due to end-replication problem	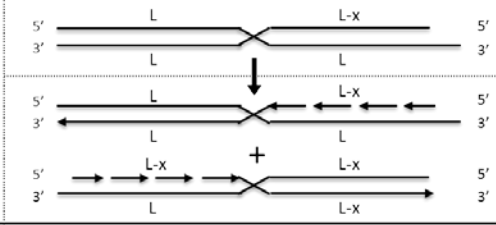	L-x/4 L-x/2	x/4
2) End-replication problem +processing of C-rich strand y=amount lost due to processing	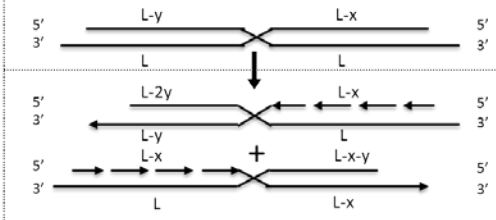	L-x/4-y/4 L-x/2-y/2	x/4+y/4
3) End-replication problem + single-strand breaks ↓ Position of single-strand breaks z=amount lost due to ssb	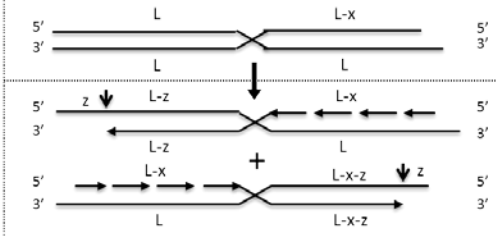	L-x/4 L-x/2-z/2	x/4+z/2
4) End-replication problem +processing of C-rich strand + single-strand breaks	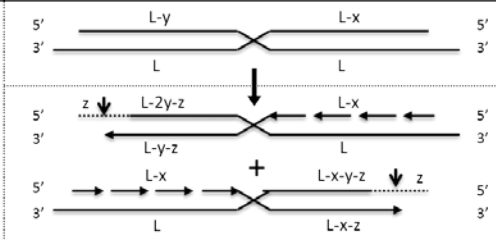	L-x/4-y/4 L-x/2-y/2-z/2	x/4+y/4+z/2

B

Cause	Proportion	Loss (nt)
incomplete end-replication	P=1	uniform distribution [10,110]
C-strand processing	P=0.8	Poisson distribution (mean 155)
single-strand breaks	$N=(10^{-8}+10^{-4}\cdot rad)t$; P=1000/10000	uniform distribution [0,1000]

Figure S1: Three mechanisms contributing to telomere shortening. (*A*) The description of telomere loss caused by each mechanism and their combinatory effects after each division. (*B*) The estimate of telomere loss induced by each mechanism.

Notably, overhangs appear at both ends of human chromosomes and there are long overhangs (over 120 nt) on about 80% of telomeres [5]. Thus, C-strand processing, represented by *y*, occurs after cell division and is simulated as a Poisson random variable with the mean of 155 nt (with a proportion of 0.8).

Single-strand breaks may occur at any time during the cell cycle and anywhere of DNA strands. The number of breaks along a telomeric DNA repeat during a cell cycle can be calculated by $N_{\text{break}} = (10^{-8}+10^{-4}rad)\ t$ with a Poisson distribution, where *rad* is the radical level of the cell and *t* is the time between cell divisions (in units of days). Under normal conditions, the cell divides every 3 days and *rad*=1000 arbitrary units [6]. Only breaks at the end of the leading strand template contribute to this loss, whereas others are repaired promptly by the cell. The probability for a break contributing to the loss is 1000/10000, and the loss, denoted by *z*, is an integer uniformly distributed between 0 and 1000. Therefore, the average loss of a telomere after a cell division is x/4+y/4+z/2=60/4+0.8×155/4+0.3×0.1×500/2=53.5 nt.

2. TRF2 couples the telomere length with the TRF2-ATM-p53-Siah1 feedback loop

On one hand, TRF2 dimers exclusively bind to the telomeric DNA repeats with different interval length and mediate DNA loop (t-loop) formation by forming a tetramer at the root [7]. T-loop is to protect the chromosome ends from degradation or fusion and from activating unwanted DNA damage signaling [8]. On the other hand, telomeric TRF2 ($TRF2_{db}$) specifically inhibits the autophosphorylation of nearby ATM on Ser1981, an indispensable step in ATM activation [9]. Thus, telomere length and the TRF2-ATM-p53 feedback loop are connected by TRF2.

TRF2 in human cells is primarily nuclear and of a primarily dimeric form [10]. Thus, we mainly consider two forms of TRF2 dimer: $TRF2_{df}$ and $TRF2_{db}$. $TRF2_{db}$ refers to functional TRF2 dimers binding the telomeric repeats to rebuild the t-loop structure, whereas $TRF2_{df}$ represents free, unbound dimers. With telomere shortening, TRF2 dimers continuously unbind telomeric DNA, namely $TRF2_{db}$ converting to $TRF2_{df}$. In the following, we derive the relationship between the concentration of TRF2 and the telomere length.

a) The reaction between TRF2 monomer ($TRF2_m$) and TRF2 dimer ($TRF2_d$) is given by

$$2[\mathrm{TRF2_m}] \underset{k_{1-}}{\overset{k_1}{\rightleftharpoons}} [\mathrm{TRF2_d}]. \tag{1}$$

At equilibrium, we have

$$[\mathrm{TRF2_d}] = \frac{k_1}{k_{1-}}[\mathrm{TRF2_m}]^2 = k[\mathrm{TRF2_m}]^2, \tag{2}$$

$$[\mathrm{TRF2}] = 2[\mathrm{TRF2_d}] + [\mathrm{TRF2_m}]. \tag{3}$$

From Eqs. (2) and (3), then

$$\begin{cases} [\mathrm{TRF2_m}] = \dfrac{\sqrt{8k[\mathrm{TRF2}]+1}-1}{4k} \\ [\mathrm{TRF2_d}] = \dfrac{1}{2}\left([\mathrm{TRF2}] - [\mathrm{TRF2_m}]\right) \end{cases}. \tag{4}$$

b) The number of TRF2 dimers is significantly greater than that of binding sites. We hypothetically use an average telomere length of 10 kbp (kilo base pair) and an interval length of 12 bp at binding sites (the telomere repeat unit is of 6 bp). Then, there are approximately 800 binding sites on a telomere, which is somewhat overestimated because the histones may well hide a number of telomeres. However, the amount of TRF2 copies in a human cell is about two millions in the nucleus [10]. Based on this gap, we make an approximation, i.e.,

$$[\mathrm{TRF2_{df}}] \doteq [\mathrm{TRF2_d}] = \frac{1}{2}\left([\mathrm{TRF2}] - [\mathrm{TRF2_m}]\right). \tag{5}$$

c) TRF2 dimers bind the telomeric DNA repeats at different intervals. We assume that there are many binding sites along telomeric repeats with a mean interval of $\Delta \boldsymbol{l}$ (in units of bp). So the number of TRF2 binding sites on a telomere, n, can be estimated by

$$n = \frac{L}{\Delta l}, \tag{6}$$

where L is the telomere length (in units of bp).

d) M is one of free binding sites, interacting with free TRF2 dimers to form a complex, $M{\cdot}\mathrm{TRF2_{db}}$, at a given forward rate. The complex in turn dissociates to free binding site and free TRF2 dimers at a given reverse rate. This dynamics can be characterized by the Michaelis-Menten kinetics:

$$[M]+[\mathrm{TRF2_{df}}] \underset{k_{2-}}{\overset{k_2}{\rightleftharpoons}} [M\bullet\mathrm{TRF2_{db}}]. \quad (7)$$

The differential rate law for the reaction is

$$\frac{d[M\bullet\mathrm{TRF2_{db}}]}{dt} = k_2[\mathrm{TRF2_{df}}][M] - k_{2-}[M\bullet\mathrm{TRF2_{db}}]. \quad (8)$$

At equilibrium, the concentrations of the species do not change, namely $d[M\cdot\mathrm{TRF2_{db}}]/dt=0$. Then,

$$\frac{[M\bullet\mathrm{TRF2_{db}}]}{[\mathrm{TRF2_{df}}][M]} = \frac{k_2}{k_{2-}} = k_e. \quad (9)$$

e) The probability for the binding site M in complex with $\mathrm{TRF2_{db}}$ can be derived from Eq. (9), i.e.,

$$\begin{aligned} P_{M\bullet\mathrm{TRF2_{db}}} &= \frac{[M\bullet\mathrm{TRF2_{db}}]}{[M]+[M\bullet\mathrm{TRF2_{db}}]} \\ &= \frac{k_e[\mathrm{TRF2_{df}}][M]}{[M]+k_e[\mathrm{TRF2_{df}}][M]} \\ &= \frac{k_e[\mathrm{TRF2_{df}}]}{1+k_e[\mathrm{TRF2_{df}}]}. \end{aligned} \quad (10)$$

f) For n binding sites like site M, the concentration of $\mathrm{TRF2_{db}}$ is given by

$$[\mathrm{TRF2_{db}}] = \frac{n}{V} P_{M\bullet\mathrm{TRF2_{db}}} = \frac{L}{\Delta l \cdot V} \frac{k_e[\mathrm{TRF2_{df}}]}{1+k_e[\mathrm{TRF2_{df}}]}, \quad (11)$$

where V is the equivalent volume.

3. p53-centered signaling network

The sensor of short telomeres. ATM acts as a sensor of short telomeres. As telomeres shorten, TRF2 dimers continuously unbind telomeres, gradually exposing the telomeric DNA to ATM. During early generations of human fibroblast, ATM is inactive as dimers. When telomeres are badly eroded, ATM dimers convert to active monomers through intermolecular autophosphorylation [11]. The process is characterized by Eqs. 1-3 in *Appendix*.

The total level of ATM is assumed to be constant since it shows no remarkable variation after DNA damage [11] (Eq. 1). ATM is divided into three forms, ATM_2 (inactive dimer), ATM (inactive monomer) and ATM_p (active monomer). Since ATM dimer is predominant at first, we set $k_{dim} >> k_{undim}$ in Eq. 2. The deactivation of ATM

by TRF2 is reflected in the $TRF2_{db}$-dependent ATM deactivation rate. Since the phosphorylation and dephosphorylation processes can be considered as enzyme-catalyzed reactions, they are characterized by the Michaelis-menten kinetics [12-14].

p53-centered feedback. Active ATM activates p53 in two manners. ATM phosphorylats p53 to disassociate it from Mdm2 and stabilizes it [15]. ATM phosphorylats Mdm2 to promote its degradation [16]. Only nuclear p53 is considered here. Two forms of Mdm2 are considered, namely $Mdm2_c$ (cytoplasmic form) and $Mdm2_n$ (nuclear form). $Mdm2_c$ is induced by $p53_p$, whereas $Mdm2_n$ targets p53 for degradation. Thus, there exists a negative feedback loop between p53 and Mdm2 [17,18].

The dynamics of p53 and Mdm2 are described by Eqs. 4-7. The phosphortylation and dephosphorylation of p53 and Mdm2 are characterized by the Michaelis-Menten kinetics. Since the ubiquitination of p53 by Mdm2 is an enzyme-catalyzed reaction, it is also described by the Michaelis-Menten form. The expression of p53-targeted genes (e.g. Mdm2) is represented by the Hill function, and the Hill coefficient is set to 4 given p53 acts as a transcription factor in a tetramer format [19]. Since $Mdm2_n$ shows a weaker binding to $p53_p$ than p53 [15], the Mdm2-dependent degradation rate of $p53_p$ is much smaller than that of p53.

Siah1 and TRF2. $p53_p$ induces the expression of *siah1*, and Siah1 targets TRF2 for proteasome-mediated degradation [20]. The dynamics of these two processes are characterized by Eqs. 8-9. As the ubiquitination of TRF2 by Siah1 is an enzyme-catalyzed reaction, it is characterized by the Michaelis-Menten kinetics.

The definition of variables and their initial values, and parameter values are presented in Tables S1 and S2, respectively. The initial concentration of each species is set to its steady-state value at adequate telomere length (i.e., 12 kb). The unit of time is minutes, while the units of parameters are set to ensure the concentrations of proteins dimensionless. The bifurcation diagrams were plotted using Oscill8.

Appendix: Equations of the model

$$[\mathrm{ATM}] = \mathrm{ATM}_{\mathrm{tot}} - 2[\mathrm{ATM}_2] - [\mathrm{ATM}_\mathrm{p}] \tag{1}$$

$$\frac{d[\mathrm{ATM}_2]}{dt} = 0.5k_{\mathrm{dim}}[\mathrm{ATM}]^2 - k_{\mathrm{undim}}[\mathrm{ATM}_2] \tag{2}$$

$$\frac{d[\mathrm{ATM}_\mathrm{p}]}{dt} = k_{\mathrm{acatm0}} + k_{\mathrm{acatm}}[\mathrm{ATM}_\mathrm{p}]\frac{[\mathrm{ATM}]}{[\mathrm{ATM}] + j_{\mathrm{acatm}}} - (k_{\mathrm{deatm0}} + k_{\mathrm{deatm1}}\frac{[\mathrm{TRF2}_{\mathrm{db}}]}{[\mathrm{TRF2}_{\mathrm{db}}] + j_{\mathrm{trf}}})\frac{[\mathrm{ATM}_\mathrm{p}]}{[\mathrm{ATM}_\mathrm{p}] + j_{\mathrm{deatm}}} \tag{3}$$

$$\frac{d[\mathrm{p53}_\mathrm{p}]}{dt} = k_{\mathrm{acp531}}[\mathrm{p53}]\frac{[\mathrm{ATM}_\mathrm{p}]}{[\mathrm{ATM}_\mathrm{p}] + j_{\mathrm{atm}}} - k_{\mathrm{dep53}}[\mathrm{p53}_\mathrm{p}] - k_{\mathrm{dp53s2}}[\mathrm{Mdm2}_\mathrm{n}]\frac{[\mathrm{p53}_\mathrm{p}]}{[\mathrm{p53}_\mathrm{p}] + j_{\mathrm{dp532}}} \tag{4}$$

$$\frac{d[\mathrm{p53}]}{dt} = k_{\mathrm{sp53}} - k_{\mathrm{dp530}}[\mathrm{p53}] - k_{\mathrm{dp532}}[\mathrm{Mdm2}_\mathrm{n}]\frac{[\mathrm{p53}]}{[\mathrm{p53}] + j_{\mathrm{dp532}}} - k_{\mathrm{acp531}}[\mathrm{p53}]\frac{[\mathrm{ATM}_\mathrm{p}]}{[\mathrm{ATM}_\mathrm{p}] + j_{\mathrm{atm}}} + k_{\mathrm{dep53}}[\mathrm{p53}_\mathrm{p}] \tag{5}$$

$$\frac{d[\mathrm{Mdm2}_\mathrm{c}]}{dt} = k_{\mathrm{smdm20}} + k_{\mathrm{smdm2}}\frac{[\mathrm{p53}_\mathrm{p}]^4}{[\mathrm{p53}_\mathrm{p}]^4 + j_{\mathrm{smdm2}}{}^4} - k_{\mathrm{dmdm2c}}[\mathrm{Mdm2}_\mathrm{c}] - k_\mathrm{i}[\mathrm{Mdm2}_\mathrm{c}] + k_\mathrm{o}[\mathrm{Mdm2}_\mathrm{n}] \tag{6}$$

$$\frac{d[\mathrm{Mdm2}_\mathrm{n}]}{dt} = k_\mathrm{i}[\mathrm{Mdm2}_\mathrm{c}] - k_\mathrm{o}[\mathrm{Mdm2}_\mathrm{n}] - k_{\mathrm{dmdm2n0}}[\mathrm{Mdm2}_\mathrm{n}] - k_{\mathrm{dmdm2n1}}[\mathrm{Mdm2}_\mathrm{n}]\frac{[\mathrm{ATM}_\mathrm{p}]}{[\mathrm{ATM}_\mathrm{p}] + j_{\mathrm{atm}}} \tag{7}$$

$$\frac{d[\mathrm{Siah1}]}{dt} = k_{\mathrm{ssiah10}} + k_{\mathrm{ssiah1}}\frac{[\mathrm{p53}_\mathrm{p}]^4}{[\mathrm{p53}_\mathrm{p}]^4 + j_{\mathrm{ssiah1}}{}^4} - k_{\mathrm{dsiah1}}[\mathrm{Siah1}] \tag{8}$$

$$\frac{d[\mathrm{TRF2}]}{dt} = k_{\mathrm{strf2}} - k_{\mathrm{dtrf21}}[\mathrm{Siah1}]\frac{[\mathrm{TRF2}]}{[\mathrm{TRF2}] + j_{\mathrm{dtrf21}}} - k_{\mathrm{dtrf20}}[\mathrm{TRF2}] \quad (9)$$

$$[\mathrm{TRF2_m}] = \frac{\sqrt{8k[\mathrm{TRF2}]+1}-1}{4k} \quad (10)$$

$$[\mathrm{TRF2_{df}}] = \frac{1}{2}([\mathrm{TRF2}] - [\mathrm{TRF2_m}]) \quad (11)$$

$$[\mathrm{TRF2_{db}}] = \frac{L}{\Delta l \cdot V}\frac{k_{\mathrm{e}}[\mathrm{TRF2_{df}}]}{1 + k_{\mathrm{e}}[\mathrm{TRF2_{df}}]} \quad (12)$$

Supplemental Table S1: Variables of the model

Variable	Description	Initial value
[ATM]	Concentration of inactive ATM monomer	0.6577
[ATM_2]	Concentration of ATM dimer	2.1622
[ATM_p]	Concentration of phosphorylated ATM monomer	0.0179
[$p53_p$]	Concentration of active p53	0.0207
[p53]	Concentration of inactive p53	0.5814
[$Mdm2_c$]	Concentration of cytoplasmic Mdm2	0.4465
[$Mdm2_n$]	Concentration of nuclear Mdm2	0.2854
[Siah1]	Concentration of Siah1	0.1001
[TRF2]	Total concentration of TRF2	3.9203
[$TRF2_m$]	Concentration of TRF2 monomer	0.4184
[$TRF2_{df}$]	Concentration of free TRF2 dimer	1.7509
[$TRF2_{db}$]	Concentration of TRF2 dimer binding to the telomeres	0.3126

Supplemental Table S2: Standard parameter values

Rate Constant	Description	Value	Reference
k_{dim}	Dimerization rate of ATM	10	[14]
k_{undim}	Dissociation rate of ATM_2	1	[14]
k_{acatm0}	Basal production rate of ATM	0.01	Estimated
k_{acatm}	Activation rate of ATM	1.9	[14]
k_{deatm0}	Inactivation rate of ATM_p	0.8	Estimated
k_{deatm1}	TRF2-dependent inactivation rate of ATM_p	2.5	Estimated
j_{acatm}	Michaelis constant of ATM activation	1	[14]
j_{trf}	Michaelis constant of $TRF2_{db}$ as a kinase	0.04	Estimated
j_{deatm}	Michaelis constant of ATM_p inactivation	2.3	[14]
ATM_{tot}	Total concentration of ATM	5	[14]
$k_{dmdm2n0}$	Degradation rate of nuclear Mdm2	0.003	[14]
$k_{dmdm2n1}$	ATM-dependent degradation rate of Mdm2	0.05	[14]
j_{atm}	Michaelis constant of ATM_p as a kinase	1	[46]
k_{acp531}	ATM-dependent activation rate of p53	0.25	Estimated
k_{dep53}	Deactivation rate of $p53_p$	0.1	Estimated
k_{dp53s2}	Mdm2-dependent degradation rate of $p53_p$	0.01	[14]
k_{sp53}	Production rate of p53	0.2	[13, 14]
k_{dp530}	Basal degradation rate of p53	0.05	[13, 14]
k_{dp532}	Mdm2-dependent degradation rate of p53	0.7	[14]
j_{dp532}	Michaelis constant of Mdm2-dependent p53 degradation	0.1	[13]
k_{smdm20}	Basal production rate of Mdm2	0.002	[14]
k_{smdm2}	p53-dependent production rate of Mdm2	0.01	Estimated
j_{smdm2}	Michaelis constant of p53-induced Mdm2 production	1	[13]
k_{dmdm2c}	Degradation rate of cytoplasmic Mdm2	0.002	[18]
k_i	Nuclear import rate of $Mdm2_c$	0.06	[13]
k_o	Nuclear export rate of $Mdm2_n$	0.09	[13]
$k_{ssiah10}$	Basal production rate of Siah1	0.01	Estimated
k_{ssiah1}	p53-dependent production rate of Siah1	0.2	Estimated
j_{ssiah1}	Michaelis constant of p53-induced Siah1 production	0.6	Estimated
k_{dsiah1}	Degradation rate of Siah1	0.1	Estimated
k_{strf2}	Basal production rate of TRF2	0.2	Estimated
k_{dtrf20}	Degradation rate of TRF2	0.05	Estimated
k_{dtrf21}	Siah1-dependent degradation rate of TRF2	0.05	Estimated
j_{dtrf21}	Michaelis constant of Siah1-dependent TRF2 degradation	1	Estimated
Δl	Mean interval length of TRF2 binding sites on telomeres	$20/V$	Estimated
V	Equivalent volume of the nucleus	$20/\Delta l$	Estimated
k_e	Equilibrium constant of TRF2 binding to telomeres	1.3	Estimated
k	Equilibrium constant of TRF2 dimerization	10	Estimated

Reference

1. Martens UM, Chavez EA, Poon SS, Schmoor C and Lansdorp PM (2000) Accumulation of short telomeres in human fibroblasts prior to replicative senescence. *Exp. Cell Res.* 256, 291-299.
2. Olovnikov AM (1996) Telomeres, telomerase, and aging: origin of the theory. *Exp. Gerontol.* 31, 443-448.
3. Wellinger RJ, Ethier K, Labrecque P and Zakian VA (1996) Evidence for a new step in telomere maintenance. *Cell* 85, 423-433.
4. von Zglinicki T (2002) Oxidative stress shortens telomeres. *Trends Biochem. Sci.* 27, 339-344.
5. Makarov VL, Hirose Y and Langmore JP (1997) Long G tails at both ends of human chromosomes suggest a C strand degradation mechanism for telomere shortening. *Cell* 88, 657-666.
6. Proctor CJ and Kirkwood TB (2002) Modelling telomere shortening and the role of oxidative stress. *Mech. Ageing Dev.* 123, 351-363.
7. Yoshimura SH, Maruyama H, Ishikawa F, Ohki R and Takeyasu K (2004) Molecular mechanisms of DNA end-loop formation by TRF2. *Genes Cells* 9, 205-218.
8. de Lange T (2002) Protection of mammalian telomeres. *Oncogene* 21, 532-540.
9. Karlseder J, Hoke K, Mirzoeva OK, Bakkenist C, Kastan MB, *et al.* (2004) The telomeric protein TRF2 binds the ATM kinase and can inhibit the ATM-dependent DNA damage response. *PLoS Biol.* 2, E240.
10. Arkus N (2005) A mathematical model of cellular apoptosis and senescence through the dynamics of telomere loss. *J. Theor. Biol.* 235, 13-32.
11. Bakkenist CJ and Kastan MB (2003) DNA damage activates ATM through intermolecular autophosphorylation and dimer dissociation. *Nature* 421, 499-506.
12. Kholodenko BN (2006) Cell-signalling dynamics in time and space. *Nat. Rev. Mol. Cell Biol.* 7, 165-176.
13. Zhang XP, Liu F and Wang W (2011) Two-phase dynamics of p53 in the DNA damage response. *Proc. Natl. Acad. Sci. USA.* 108, 8990-8995.
14. Ma L, Wagner J, Rice JJ, Hu W, Levine AJ, et al. (2005) A plausible model for the digital response of p53 to DNA damage. *Proc. Natl. Acad. Sci. USA.* 102, 14266-14271.
15. Prives C (1998) Signaling to p53: breaking the MDM2-p53 circuit. *Cell* 95, 5-8.
16. Stommel JM and Wahl GM (2004) Accelerated MDM2 auto-degradation induced by DNA-damage kinases is required for p53 activation. *EMBO J.* 23, 1547-1556.
17. Wu X, Bayle JH, Olson D and Levine AJ (1993) The p53-mdm-2 autoregulatory feedback loop. *Genes Dev.* 7, 1126-1132.

18. Wee KB and Aguda BD (2006) Akt versus p53 in a network of oncogenes and tumor suppressor genes regulating cell survival and death. *Biophys. J.* 9, 857-865.

19. Jeffrey PD, Gorina S and Pavletich NP (1995) Crystal structure of the tetramerization domain of the p53 tumor suppressor at 1.7 angstroms. *Science* 267, 1498-1502.

20. Fujita K, Horikawa I, Mondal AM, Jenkins LM, Appella E, *et al*. (2010) Positive feedback between p53 and TRF2 during telomere-damage signalling and cellular senescence. *Nat. Cell Biol.* 12, 1205-1212.